Universal Stress-Sensing Dimeric Anthracene-Based Mechanophore Particle Fillers Incorporated into Polyurethane Thermoset Matrices

Elizabeth M. Nofen, Avi Dasgupta, Nicholas Zimmer, Ryan Gunckel, Bonsung Koo, Aditi Chattopadhyay, Lenore L. Dai

School for Engineering of Matter, Transport and Energy, Arizona State University, Tempe, Arizona 85287

Mechanochemistry, in which mechanical forces induce chemical changes, can allow for targeted damage detection by way of embedded mechanophore units, which emit a measurable signal change correlating to an applied force. In this work, we successfully created stress-sensing, functional composites by employing microparticles of the mechanophore dimeric 9-anthracene carboxylic acid in a thermoset polyurethane matrix. The goal being to study the application of the particles as universal stress-sensing fillers in network polymer matrix composites, after previously evaluating the particles in an epoxy matrix. Under a compressive force, there is bond breakage in the mechanically weak cyclooctane photodimers, such that there is reversion to the fluorescent anthracene-type monomers. This fluorescent emission was then correlated to the applied strain, and the precursors to damage were detected with a noticeable signal change at a strain of only 2%, which was attributed to increased interactions between the matrix and the particles, with possible surface grafting occurring. This early damage detection was additionally possible at very low particle loadings of 2.5 and 5 wt%, with the 5 wt% loading showing enhanced material properties, due to particle reinforcement. Overall, the stress-sensitive particle filler allows for facile addition of advanced functionality to these ubiquitous thermoset composites. POLYM. ENG. SCI., 57:901–909, 2017.

INTRODUCTION

Composites are materials consisting of two or more differing components, and have been ubiquitous to human life, ever since straw and mud were first mixed to form crude bricks for building construction [1]. This guiding principle has made the use of composites not limited to building materials, but has opened up their use to a myriad of applications, including electronics and optics [2–7], membranes, medical devices and biological research [8–13], catalysis [14–17], energy harvesting and storage [18–24], among a multitude of others. In particle-reinforced composites (PRCs), a matrix is reinforced by particle fillers, and the nearly unlimited combination of filler and matrix type allow for a wide variety of composite material properties and applications [25–28].

Mechanochemistry is the area of chemistry that involves the use of mechanical force to induce a chemical change, separate from the other well-studied areas of thermochemistry, electrochemistry, and photochemistry [29]. Mechanochemistry offers alternative routes to obtain desired products, as the use of mechanically active groups can allow for unconventional reaction pathways [30–33]. The use of mechanophores, which are molecular units that change chemically in response to an applied force, can allow for novel damage detection schemes through their ability to act as stress sensors in various polymer matrices, forming the field of polymer mechanochemistry [34–38]. In terms of mechanophores operating by the phenomenon of cycloreversion, cyclobutane-based mechanophores have been well studied due to the intrinsic fluorescence of the mechanophore precursors, the loss of this fluorescence after dimerization, and the reappearance of the fluorescent signal after an applied force [39–42]. In addition, cyclopropane has been used as a mechanophore due to the greater strained nature of the ring, generally following an electrocyclic ring opening mechanism due to the small structure of the ring [43, 44]. Anthracene, consisting of three fused benzene rings, is a commonly used fluorophore due to its strong fluorescent signal and ease of incorporation into different molecular structures due to its carboxylic acid and other derivatives [45, 46]. Its large conjugated structure also allows for its incorporation into many optical-driven fields, including liquid crystals [47]. Upon application of UV light, anthracene derivatives can photodimerize into a number of structures, with resulting applications in shape memory [48], self-healing [49], and the study of mechanochemical activation [50–54]. Anthracene has a much higher absolute fluorescence quantum yield compared with other mechanophores, due to its large conjugated system, and thus it is a desirable candidate for mechanochemical signaling via fluorescence generation [55].

Polymer mechanochemistry using mechanophores as stress sensors is a relatively new field, and it is worthwhile to note that the previously mentioned mechanophore studies exclusively involve solutions, thin films, or elastomeric/thermoplastic matrices, thus creating a notable gap in the literature concerning thermoset network polymer systems and engineering composites. There have only been a handful journal articles involving the incorporation of mechanophores into a polyurethane matrix, specifically spiropyran, dioxetane, oxanorbornadiene, diarylbibenzofuranone, and rhodamine, and all used thermoplastic/elastomeric polyurethane, rather than a thermoset [56–61]. In elastomeric systems, the samples typically must be stretched to 100% or more of their initial length to activate the incorporated mechanophores, whereas we desire early damage detection of in the vicinity of the yield point, which can be less than 4% strain in our systems. Polyurethane is an important engineering polymer, due to its robust chemical and physical properties, and the tunability of these properties by varying the chosen chemistries. Elastomeric/thermoplastic polyurethane can additionally be synthesized to contain soft (long chain polyol) and hard (diisocyanate groups and a chain extender) segments, and covalent mechanophore incorporation into these segments has been

Correspondence to: L.L. Dai; e-mail: lenore.dai@asu.edu

Contract grant sponsor: Army Research Office; contract grant number; W911NF1510072.

DOI 10.1002/pen.24467

Published online in Wiley Online Library (wileyonlinelibrary.com).

shown to be successful previously [57, 58, 60]. However, the particle incorporation method described in this work is synthetically more facile, as it simply involves mixing the mechanophore particles with the two parts of the polyurethane system to yield a PRC with additional stress responsive capabilities.

In our early work, we created self-sensing polymer blends of cyclobutane-based mechanophores and epoxy [62]. The polymer blend scheme allowed for early damage detection, however, poor thermal and mechanical properties resulted from the simple blending formation mechanism. Thus, we continued our study by synthesizing dimeric anthracene-based mechanophore particles as novel mechanophores in epoxy composites [63]. The particles were able to achieve damage precursor detection in the epoxy matrix, thus in this work, we sought to prove the use of these novel particles as universal stress-sensitive particles in thermoset matrices regardless of the matrix chemistry. In addition, this is the first study of an anthracene-functional mechanophore in a polyurethane matrix, with the added novelty of the first study of a particle mechanophore in a polyurethane matrix.

EXPERIMENTAL

Materials

9-Anthracene carboxylic acid (AC, Alfa Aesar), tetrahydrofuran (THF, Alfa Aesar), and deuterated dimethyl sulfoxide (DMSO-d_6, Cambridge Isotope Laboratories) were used as received. The thermoset polyurethane (PU) matrix used was Crystal Clear ® 200 from Smooth-On, Inc. which consisted of 4,4′-methylenedicyclohexyl diisocyanate (Part A) and a proprietary polyol (Part B).

Dimeric 9-Anthracene Carboxylic Acid (Di-AC) Synthesis and Characterization

To form dimeric 9-anthracene carboxylic acid (Di-AC) particles, 2 g of AC was mixed with 40 mL of THF under magnetic stirring, a nitrogen purge, and subsequently exposed to a 302 nm wavelength UV lamp (UVP, UVM-28), with a light density of approximately 1,300 μW cm^{-2} at a distance of 3 cm, for three days. The white Di-AC precipitate was washed with THF by gravity filtration and then vacuum dried to remove excess solvent, with a yield of 31%. The Di-AC product was then filtered through 10 μm filter paper (EMD Millipore) with acetone to gather particles under 10 μm, and to ensure a uniform particle size. The particles were subsequent dried in a vacuum oven to remove excess solvent. ^{1}H NMR (400 MHz, DMSO-d_6) δ 13.52 (2H, s), 6.85–6.74 (24H, m), 5.59 (2H, s).

^{1}H Nuclear Magnetic Resonance (NMR) spectra were taken with a Bruker 400 MHz NMR spectrometer. Fourier Transform Infrared (FTIR) spectra were taken under vacuum in a Bruker IFS 66v/S FTIR spectrometer equipped with a Pike Diamond ATR (Attenuated Total Reflectance) accessory. The particle size of a dilute solution of Di-AC in THF was determined via Dynamic Light Scattering (DLS) with a PSS NICOMP 380 ZLS. The chemical structures of AC and Di-AC were drawn with MarvinSketch.

Mechanophore-Embedded Polyurethane Composite Preparation and Characterization

To form the composites consisting of 2.5 and 5 wt% Di-AC particles in a thermoset polyurethane matrix, the 10 μm filtered Di-AC particles and 4,4′-methylenedicyclohexyl diisocyanate (Part A) were mixed with an impeller mixer at 200 rpm for 5 min at room temperature so that the particles were dispersed. The proprietary polyol (Part B) was then added to the diisocyanate/Di-AC mixture at a mass ratio of $M_{\text{Part A}}$:$M_{\text{Part B}}$ = 10:9, and mixed with the impeller mixer at 200 rpm for 5 min again at room temperature. After the mixture was homogenous, it was poured into silicone rubber molds and degassed in a vacuum oven at −29 in Hg for 90 min. The polyurethane was then allowed to cure overnight at room temperature, and then post cured at 70°C for 8 h. Neat polyurethane samples were prepared in a similar manner at the same 10:9 mass ratio. After simple machining, the average dimensions of the samples for the compression test were 3 mm × 4 mm × 8 mm and 2 mm × 12 mm × 35 mm for the Dynamic Mechanical Analyzer (DMA) tests. 1,000 nm sections of the composites were made with a Leica Ultracut R Microtome, which were then observed under a Leica SP5 confocal laser-scanning microscope to evaluate the particle size of the composites under transmitted light.

A TA Instruments Q20 Differential Scanning Calorimeter (DSC) was used to determine the glass transition temperature (T_g) of the polyurethane samples under nitrogen in aluminum Tzero pans with lids, with air (an empty pan and lid) used as the reference. A heat/cool/heat procedure was used in which the sample was first heated to 70°C to eliminate any thermal history, cooled to −20°C, and then heated to 120°C to determine the T_g, with 10°C/min as the heating and cooling rates. A TA Instruments Thermogravimetric Analyzer (TGA) Q500 was used to determine the decomposition temperatures (T_d) by heating from 25°C to 600°C at a heating rate of 10°C min^{-1} under nitrogen, with aluminum sample pans. The multi-frequency/strain method of a TA Instruments Q800 Dynamic Mechanical Analyzer (DMA) was used to further evaluate the thermal and mechanical properties of the composite samples with the single cantilever clamp and a frequency of 1 Hz under amplitude control. The strain amplitude was set at 25 μm and the temperature was ramped from 25°C to 120°C at a heating rate of 5°C/min. The characteristic temperatures and moduli values from DSC, TGA, and DMA were found using the built in functions in the TA Instruments Universal Analysis software. A TestResources 800L Compression Test System was used to compress the samples to different strains and obtain stress–strain curves. Unwanted shearing was prevented by using a small amount of petroleum jelly on samples to minimize their friction with the compression plates. The tests were run in displacement control in the longitudinal direction at a loading rate of 1 mm/min and the tests were conducted at room temperature. The fluorescence generation from the compressed polyurethane samples was observed under a Nikon Eclipse TE300 inverted video fluorescence microscope, by excitation under 340–380 nm UV light, with a filter cube to capture the emission of light between 435–485 nm. All images were taken with a black-and-white camera and with the same intensity of light, gain, and exposure time. The Image J (http://imagej.nih.gov/ij/) software package was used to quantify the fluorescence intensity of the images taken. Every image was first converted to an 8-bit image and then the "Measure" function was used to calculate the integrated intensity for the selected area of the image; this is through the software taking the sum of the pixel values in the image, and then averaging the intensity at each point. The 8-bit gray scale

 DOI 10.1002/pen

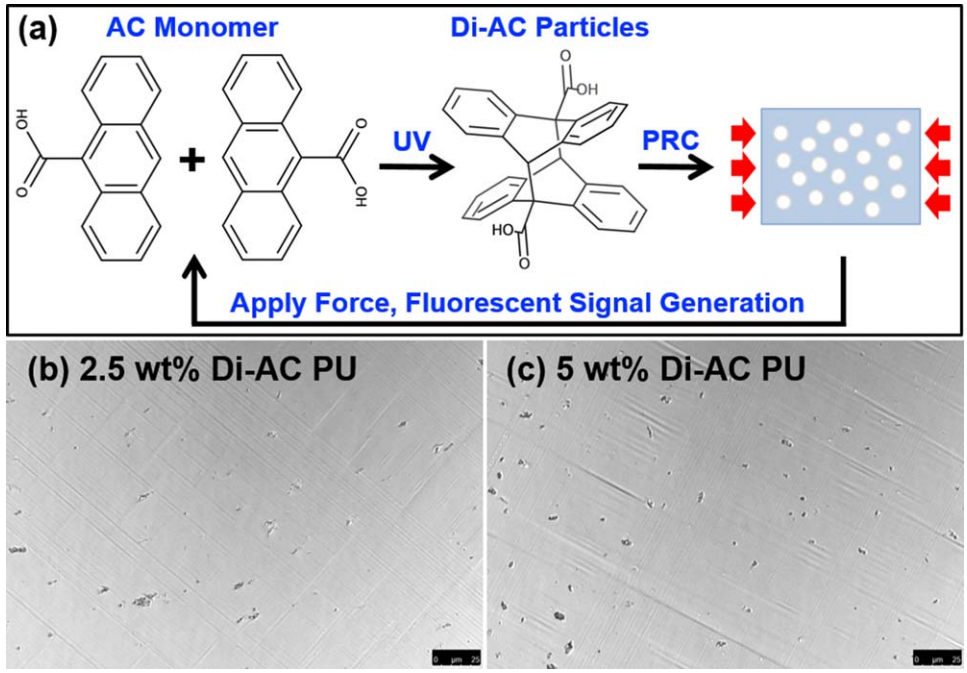

FIG. 1. The top schematic shows an overview of the study, including photodimerization of the fluorescent AC monomer to the Di-AC particle mechanophore, followed by incorporation of the particles into a polyurethane matrix, with subsequent compression for the fluorescent mechanochemical activation. The bottom two confocal microscopy images show microtome sections of both the 2.5% and 5% Di-AC polyurethane composites to show the dispersion of the particles within the matrix. The scale bars are 25 μm. [Color figure can be viewed at wileyonlinelibrary.com]

fluorescence images from the fluorescence microscope were pseudocolored green with ImageJ with the built-in "Green" LUT, and the fluorescent images published in this paper were further enhanced by increasing both the brightness and contrast by 40% for better visualization of the fluorescence change.

RESULTS AND DISCUSSION

Formation and Material Properties of the Di-AC Embedded PU Composites

9-Anthracene carboxylic acid (AC) was photodimerized in solution under UV light via [4 + 4] cycloaddition to form cyclooctane-type rings, with prominently head-to-tail structures [64]. A schematic of this reaction to form the dimerized 9-anthracene carboxylic acid (Di-AC), which can be recovered as a pure white powder, can be seen in Fig. 1. Di-AC is a known mechanophore, with its cyclooctane-type dimer reverting back to the fluorescent anthracene form under an applied force [50, 63]. In this work, the recovered Di-AC powered was filtered through 10 μm filter paper to remove any large aggregates and capture Di-AC particles of a micro-scale particle size. Dynamic light scattering (DLS) determined the particle size to have a Gaussian distribution for the diameter at 1,512 ± 1,328 nm. Figure 1 also shows the incorporation of the Di-AC particles into a polyurethane matrix for fluorescent stress sensing under compression. The bottom two confocal microscopy images of Fig. 1 show 1,000 nm microtome sections of both the 2.5% and 5% Di-AC polyurethane composites, and the dispersion of the particles within the matrix can be seen. To form the mechanophore-embedded polyurethane composites, the Di-AC particles were first impeller mixed with the diisocyanate so that it would be evenly dispersed throughout the composite. The polyol was then impeller mixed into the diisocyanate-particle mixture to obtain a final homogenous mixture. This mixture was then poured into rubber molds, vacuum degassed, cured at room temperature overnight, following by thermal post curing. The compositions of 2.5% and 5 wt% Di-AC in the composites was chosen as these were the least amounts of mechanophore that could be used to still generate the desired stress sensing signal. The least amount of mechanophore was desired as incorporating the particles into polyurethane interrupts the network formed between the diisocyanate and polyol when the polyurethane cures, impacting the resulting thermal and mechanical properties of the composites.

Figure 2 shows the ATR-FTIR spectra of the pure Di-AC power mechanophore, the neat polyurethane, and the 2.5 and 5 wt% Di-AC PU composites to evaluate the chemical interaction between the Di-AC particles and the polyurethane matrix. The use of ATR-FTIR allows for some quantitative analysis of the peak heights generated as the entirety of the light passing through the sample and the ATR diamond is able to be detected. As polyurethane forms its thermoset crosslinked network by the reaction of diisocyanate groups with hydroxyl groups, it can be hypothesized that the diisocyanate groups can react with the —OH on the free carboxylic acid groups in Di-AC. As Di-AC is in a microparticle form, likely held together by hydrogen bonding between its molecules, the free carboxylic acid sites that could react with the diisocyanate groups would be on the surface of the particles.

Even if only a portion of the carboxylic acid groups reacted with the polyurethane matrix, this covalently embedding of the particles into the matrix could enhance the particles mechanochemical response, as the deformation of the matrix could more readily be transferred to the particles and interfacial effects would be lessened. The FTIR spectra in the inset of Fig. 2 show

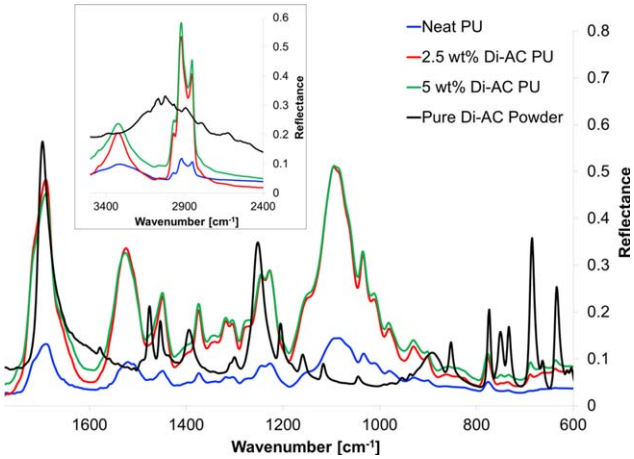

FIG. 2. ATR-FTIR spectra of the pure Di-AC power mechanophore (black), the neat polyurethane (blue), and the 2.5 and 5 wt% Di-AC PU composites (red and green, respectively), with the main image being the range of wavenumbers from 1,700 to 600 cm^{-1} and the inset being the range of wavenumbers from 3,500 to 2,400 cm^{-1}. [Color figure can be viewed at wileyonlinelibrary.com]

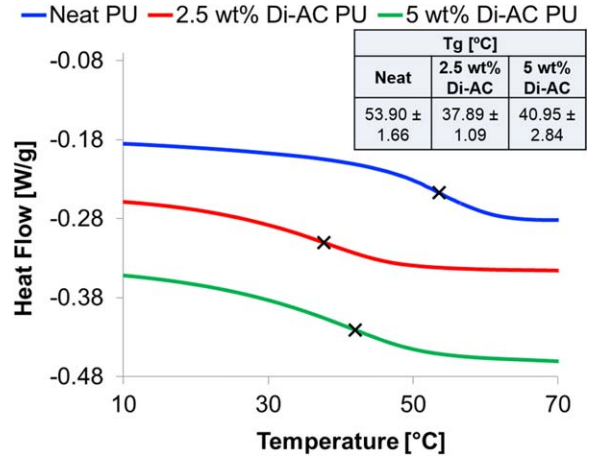

FIG. 3. Representative DSC scans showing the glass transition for the neat polyurethane (blue) and the 2.5 and 5 wt% Di-AC PU composites (red and green, respectively), with the resulting T_g values (as an average of 4 runs) inset on the top right. [Color figure can be viewed at wileyonlinelibrary.com]

this behavior, as the broad carboxylic acid —OH peak seen in Di-AC from 3,400–2,400 cm^{-1}, is not seen in the Di-AC composite spectra, providing evidence that at least some of the Di-AC carboxylic acid groups have reacted with the matrix [65, 66]. In this region, it can additionally be seen that the intensities of the alcohol —OH peak near 3,317 cm^{-1} and the alkane C—H peaks from 3,000–2,800 cm^{-1} have been increased upon addition of the Di-AC particles. In the main image in Fig. 2, multiple characteristic peaks can be observed, including the enhancement of the C═O peak near 1,695–1,685 cm^{-1} with addition of the Di-AC particles, and the strong aromatic peaks at 685 and 633 cm^{-1} in the Di-AC spectra, not present in the neat polyurethane spectra, being faintly incorporated into the composite Di-AC PU spectra. In general, all peaks present in the neat polyurethane spectra had an increased intensity when the Di-AC particles were added.

The thermal and mechanical properties of the Di-AC embedded composites were then obtained to determine the effect of adding the mechanophore on these properties. Differential Scanning Calorimetry (DSC) was used to determine the glass transition temperature (T_g) of the various samples. Representative DSC scans for the neat and Di-AC polyurethane composites can be seen in Fig. 3. The average T_g values over 4 runs were 53.90 ± 1.66°C, 37.89 ± 1.09°C, and 40.95 ± 2.84°C, for the neat, 2.5 wt% Di-AC, and 5 wt% Di-AC polyurethane samples, respectively. This results in a decrease of the T_g from the neat of approximately 13°C–16°C for 5 and 2.5 wt% particle addition, respectively. This T_g depression can be expected as the particles interrupt the thermoset network formation.

Figure 4 shows representative Thermogravimetric Analysis (TGA) for the samples, with the corresponding Differential Thermal Gravimetry (DTG) curves in the inset left. These tests were run under nitrogen to eliminate weight loss due to oxidation, and thus capture the thermal decomposition of the bonds within the polyurethane samples. The main decomposition temperatures (T_d) were found via the peaks in the DTG curves, and were 352.02 ± 1.74°C, 350.92 ± 1.26°C, and 352.41 ± 2.92°C, for the neat, 2.5 wt% Di-AC, and 5 wt% Di-AC polyurethane samples, respectively. These values are not statistically different from each other, thus the addition of the mechanophore particles did not significantly change the T_d. It is worthwhile to note that the main T_d of the pure Di-AC powder (prior to embedding) was found to be 244.50 ± 1.83°C, which is relatively high and likely contributed to the particle addition not significantly affecting the T_d of the embedded composite.

Dynamic Mechanical Analysis (DMA) can be used in addition to DSC to determine T_g values, as well as determine the crosslink density of the polyurethane samples (Fig. 5). The DMA measures the storage and loss moduli of a sample by physical oscillation, with the ratio of the two moduli being defined as tan delta (tan δ). The peak of the tan δ curve is then used to determine the T_g value for the sample. From DMA, the T_g values over 4 runs of each sample were 75.34 ± 1.50°C, 65.30 ± 2.71°C, and 67.46 ± 2.15°C, for the neat, 2.5 wt% Di-AC, and 5 wt% Di-AC polyurethane samples, respectively. This makes for an approximate depression of the T_g by 10°C and 8°C for the 2.5 and 5 wt% Di-AC composites from the neat, respectively. It should be noted that this depression is

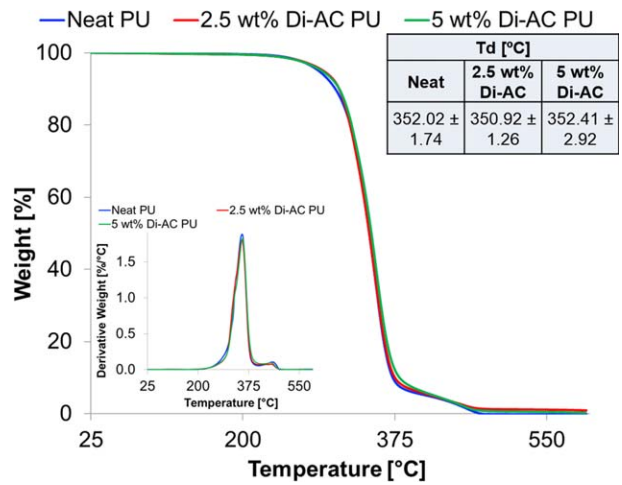

FIG. 4. Representative TGA curves showing the thermal decomposition of the neat polyurethane (blue) and the 2.5 and 5 wt% Di-AC PU composites (red and green, respectively), with the resulting T_d values (as an average of 4 runs) inset on the top right. [Color figure can be viewed at wileyonlinelibrary.com]

DOI 10.1002/pen

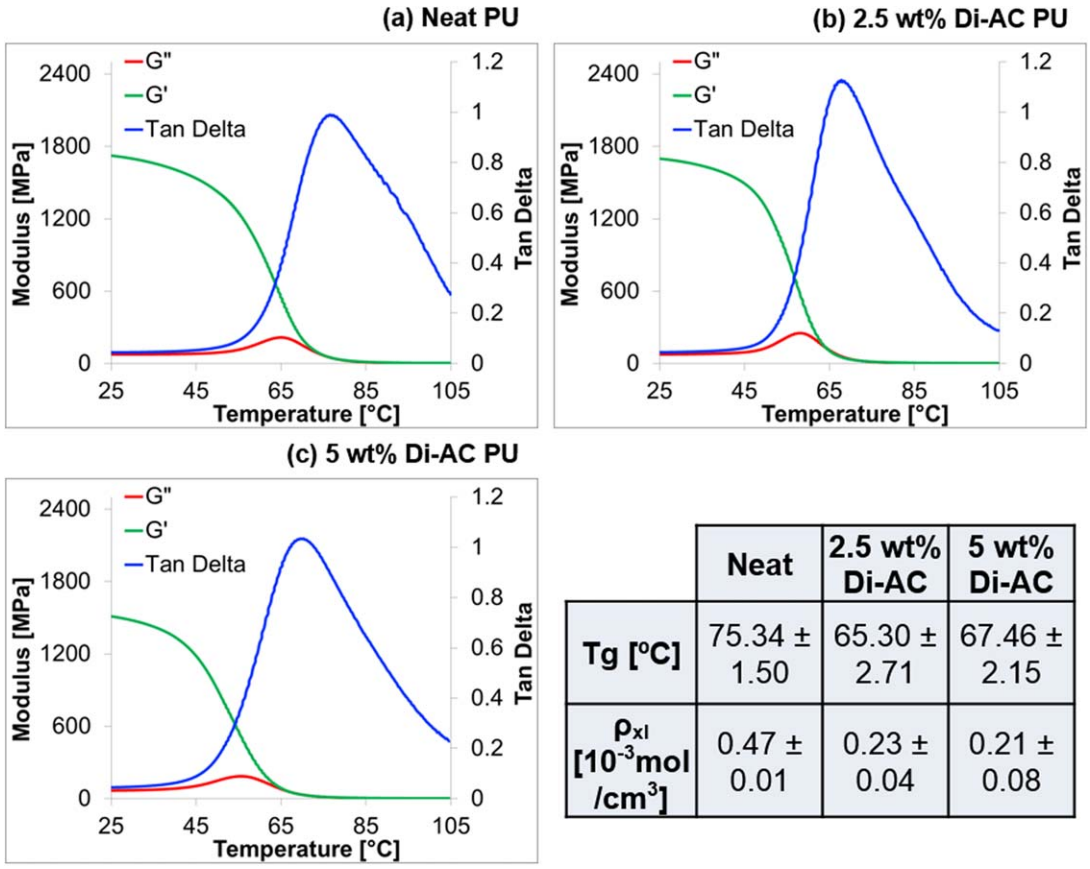

	Neat	2.5 wt% Di-AC	5 wt% Di-AC
Tg [°C]	75.34 ± 1.50	65.30 ± 2.71	67.46 ± 2.15
ρ_{xl} [10^{-3}mol/cm^3]	0.47 ± 0.01	0.23 ± 0.04	0.21 ± 0.08

FIG. 5. DMA curves showing the Storage Modulus (G', green), Loss Modulus (G'', red), and Tan Delta (blue) of the (a) neat polyurethane, (b) 2.5 wt% Di-AC composite, and (c) 5 wt% Di-AC composite, respectively. The inset table shows the average T_g and ρ_{xl} of the samples determined from the DMA curves. [Color figure can be viewed at wileyonlinelibrary.com]

slightly less than what was seen with the DSC, and that all of the T_g values are greater with the DMA compared with the DSC. In addition, there was an approximate 2°C increase in the T_g for the 5 wt% Di-AC PU compared with the 2.5 wt% Di-AC PU. These results can be hypothesized to be from the mechanical determination of the T_g in DMA, rather than the thermal determination in DSC. This mechanical determination then can allow for some small particle reinforcement behavior in the 5 wt% value that was not seen in the DSC measurements. To calculate the crosslink density, the theory of rubber elasticity can be utilized [67], $\rho_{xl}=G'/3RT$, where ρ_{xl} is the crosslink density expressed in moles of elastically effective network chains per cm^3 of sample, G' is the rubbery plateau modulus, R is the Gas Constant, and T is the absolute temperature at which the rubbery plateau modulus is determined. The crosslink densities were thus calculated to be $0.47 \pm 0.01 \times 10^3$, $0.23 \pm 0.04 \times 10^3$, and $0.21 \pm 0.08 \times 10^3$ mol/cm^3, for the neat, 2.5 wt% Di-AC, and 5 wt% Di-AC polyurethane samples, respectively. Thus, there was a significant decrease in the crosslink density upon addition of the Di-AC particles due to the disruption of the polyurethane network formation.

Mechanochemical Fluorescence Signal Generation for Damage Precursor Detection

A compressive force was used to apply measurable and repeatable damage to the thermoset polyurethane samples, and certain strain values were chosen to determine the resulting mechanochemical response. From these compression tests, stress–strain curves of the neat and composite polyurethane samples were generated to identify whether certain strain values were in the elastic or plastic deformation region of the curve, and to evaluate the change in the mechanical properties after Di-AC particle incorporation. Figure 6 shows the resulting stress–strain curves for all three sample types. The Young's modulus values in the linear elastic region of the curve were found to be 1.48 ± 0.02, 0.97 ± 0.10, and 1.27 ± 0.09 GPa for the neat, 2.5 wt% Di-AC, and 5 wt% Di-AC polyurethane samples, respectively. Thus, there was a notable decrease in the Young's modulus upon 2.5 wt% particle addition, but recovery of some of this loss upon increasing the particle content to 5 wt%. Similarly, the yield strength values were 62.19 ± 0.30, 39.08 ± 0.78, and 50.93 ± 0.16 MPa for the neat, 2.5 wt% Di-AC, and 5 wt% Di-AC polyurethane samples, respectively. The depression of the Young's modulus and yield strength values can be attributed to the particles disrupting the polyurethane network, however, when 5 wt% particles are added, there is some particle reinforcement behavior, and thus some recovery of the mechanical properties.

The selected strain values from the compression tests for the fluorescence imaging were 0%, 2%, 4%, 6%, 10%, and 15%, and representative images for these strains for both the 2.5 and 5 wt% Di-AC composites can been seen in Fig. 7a and b, respectively. These images were taken under excitation of 340–

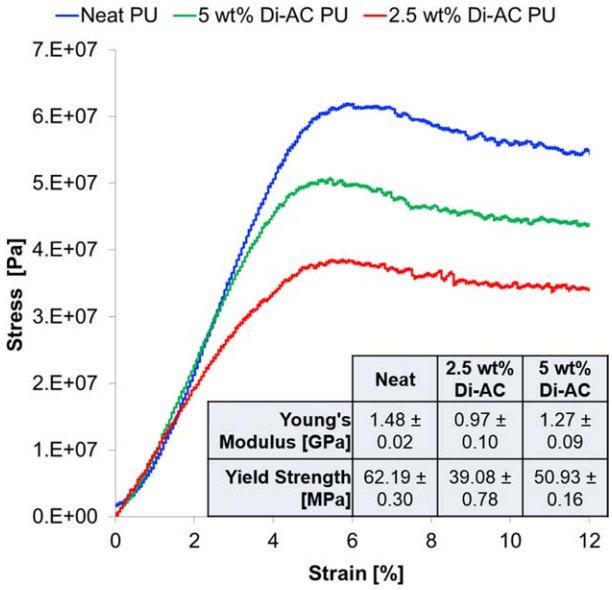

FIG. 6. Stress–strain curves for the neat polyurethane (red) and the 2.5 and 5 wt% Di-AC PU composites (red and green, respectively), with the lower right inset showing the resulting Young's Modulus and Yield strength values. [Color figure can be viewed at wileyonlinelibrary.com]

380 nm UV light, with a filter cube to capture the light emission between 435–485 nm. The 8-bit gray scale fluorescence images from the microscope were subsequently pseudocolored green with the built-in "Green" LUT in ImageJ, and all of the images seen in Fig. 7 were further enhanced by increasing both the brightness and contrast by 40% for better visualization of the increase in fluorescence with an increase of the strain applied. Correlating the selected strain values seen in Fig. 7 with the compression test curves, 0% strain is prior to compression, to provide a baseline for the testing, and 2% and 4% strain are in elastic region, with 2% in the approximate middle of the region and 4% immediately before the yield point. 6% strain is immediately after the yield point, and 10% and 15% strain are well into the plastic region. Comparing each strain value between the 2.5 and 5 wt% Di-AC composites, it can be seen that the 5 wt% Di-AC composite has slightly higher fluorescent emission overall compared with the 2.5 wt%, which is expected as some baseline fluorescence exists for the Di-AC mechanophore on its own, thus using more of it increases the overall fluorescence. For both weight percents studied, an obvious increase in the fluorescence for the 2% compared with the 0% strain can be seen visually, and this fluorescent increase can be seen with the increasing applied strain. This visualization of the fluorescence change at 2% is a form of very early damage detection, as 2% strain is firmly in the elastic region of the stress–strain curve. In addition, for 2.5 wt% Di-AC, in the 0% and 2% strain images, individual particles are not seen, but with the 4% strain and above, clear activated particle aggregates can be observed, along with the overall increase in the background fluorescence. For the 5 wt% Di-AC, particle aggregates can be faintly observed in the 0% strain image, with their fluorescence increasing over the applied strain. This difference is simply due to the increase in particles used in the 5 wt% composite compared with the 2.5 wt% composite.

To fully evaluate the functionality of the synthesized mechanophore-embedded composites for damage precursor detection, quantification of the change in the fluorescence intensity with the applied strain was required, and can be seen in Fig. 8. To quantify the fluorescence intensity at each of the studied strain values, the "Measure" function in ImageJ was used on the raw 8-bit grayscale images obtained from the fluorescence microscope. The ImageJ software generated an average fluorescence intensity value for each of the images by taking the sum of the pixel values in the image and then averaging the intensity at each point. At each of the selected strain values from the compression tests, eight fluorescence microscopy images were taken for each sample, representative of the entire sample face. Four samples were used per each strain value (2 each from 2 separate composite batches), thus each point seen in Fig. 8 is the average of 32 fluorescence images with the corresponding standard deviation values. Reinforcing the qualitative trend seen with the fluorescence images in Fig. 7, Fig. 8 clearly shows the enhancement in fluorescence with applied strain for both the 2.5 and 5 wt% Di-AC composites.

The inset of Fig. 8 shows the raw fluorescence intensity values calculated from ImageJ, and it can be seen that the 5 wt% Di-AC composite indeed has a higher overall fluorescence, due to the increased amount of particles used. For both weight percents used, there is a marked increase in the fluorescence intensity between 0% and 2% strain, with a lesser increase when moving up to 4% and 6% strain, leveling off after the 6% strain. This extreme increase in the observed fluorescence after only 2% strain shows this system's capability for damage precursor detection, in which the sample has not been irreversibly deformed at all, but the clear fluorescent signal is present, even with a very low mechanophore particle concentration of 2.5 wt%. In our previous work with Di-AC in epoxy, 5 wt% of the Di-AC particles were required to observe the mechanophore activation, and there was not such a clear signal at 2%, with 4% identified as the early damage detection point [63]. In addition, the epoxy and polyurethane systems had similar starting fluorescence values comparatively, so it is hypothesized that this increase in the fluorescent signal observed is due to some interaction with the Di-AC particles in polyurethane rather than epoxy, as discussed for the FTIR spectra for the Di-AC polyurethane composites in Fig. 2 of this work. This is likely due to the possibility of some of the carboxylic acid groups on the surface of the Di-AC particles being able to react with the diisocyanate groups of the polyurethane, while the epoxide-amine reaction in epoxy is favored over reaction of the Di-AC carboxylic acid groups and the epoxide rings [68]. Covalent bonding of the particles to the polyurethane matrix would then cause an increased fluorescence response as any deformation to the matrix would be more efficiently transferred to the stress-sensitive particles, and interfacial effects would be lessened. The main chart of Fig. 8 shows the overlay of the 2.5 and 5 wt% Di-AC polyurethane curves by normalizing both curves to their respective 0% strain values, and there is very good agreement for all values between the two weight percents, especially for the 2% strain. This analysis shows that this behavior is intrinsic to the Di-AC particle mechanophore used, and not dependent on the weight fraction of particles. However, while the used of the lesser value of 2.5 wt% is appealing, the reduction in the thermal and mechanical properties of these composites makes the use of the 5 wt% composites more desirable, as the damage detection functionality is

DOI 10.1002/pen

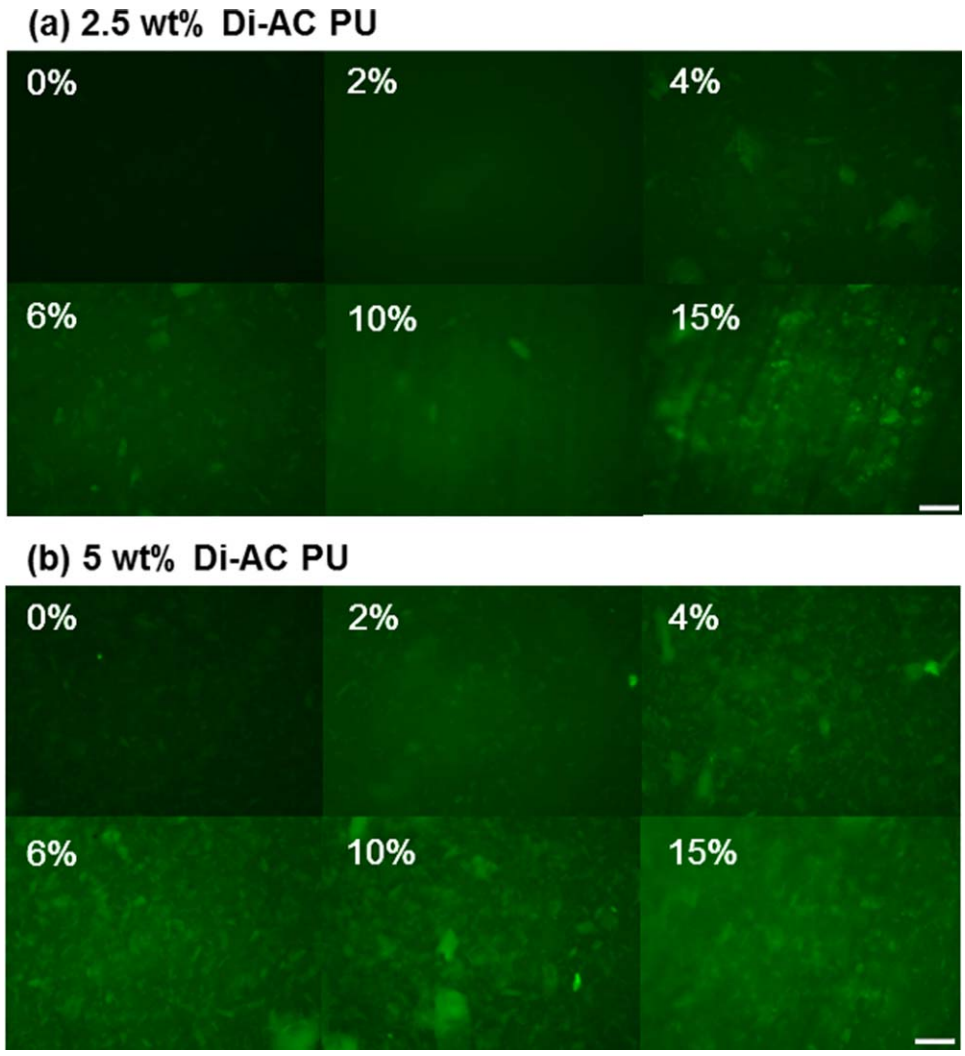

FIG. 7. Representative fluorescence images for the mechanophore-embedded polyurethane composites identifying the strain values for which the images were taken, for (a) 2.5 wt% Di-AC and (b) 5 wt% Di-AC. Scale bars are 50 μm. The images were pseudocolored green and the brightness and contrast were increased by 40% to enhance the visual analysis of the images. [Color figure can be viewed at wileyonlinelibrary.com]

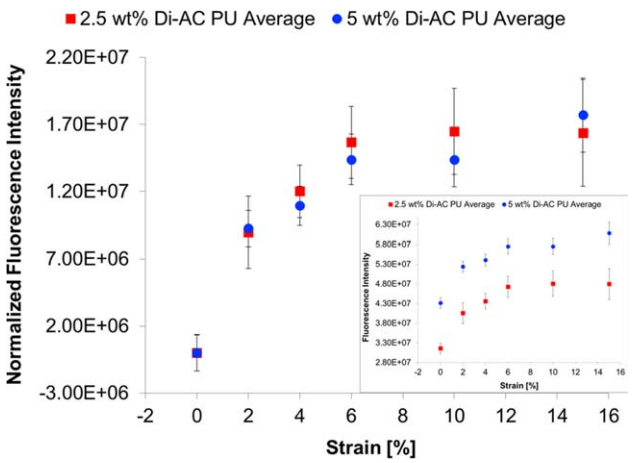

FIG. 8. (a) Average fluorescence intensity values for each strain value calculated via ImageJ, for the 2.5 and 5 wt% Di-AC PU composites (red and blue, respectively). Each fluorescence intensity value was averaged over 32 pictures for each strain. (b) By normalizing both curves to the 0% strain value, the overlaying of the curves shows the same trend regardless of the weight fraction of Di-AC used. [Color figure can be viewed at wileyonlinelibrary.com]

present with a comparative increase of the thermal and mechanical properties.

CONCLUSIONS

The study of mechanochemistry focuses on mechanical forces inducing a chemical change, and can allow for targeted damage detection by way of embedded mechanophore units, with can emit fluorescent signals in response an applied force. However, anthracene derivatives, including the force-responsive ones, have previously only been studied in solution, films, or elastomers; leaving room open for their novel application in other material schemes, including engineering composites. In this work, we successfully employed microparticles of the mechanophore dimeric 9-anthracene carboxylic acid (Di-AC) in a thermoset polyurethane matrix to study their application as universal stress-sensing fillers in network thermoset polymer matrix composites. Under a compressive force, there was bond breakage in the mechanically weak cyclooctane photodimers of Di-AC, such that there is reversion to the fluorescent anthracene-type monomers. This fluorescent

emission was then correlated to the applied strain, and the precursors to damage were detected with a noticeable fluorescent signal change at an applied strain of only 2%. The underlying mechanisms regarding this very early detection were probed and hypothesized to be due to enhanced interactions of the particles with the matrix, with possible surface grafting of the mechanophore particles to the polyurethane matrix. This early damage detection was additionally possible at very low particle loadings of 2.5 and 5 wt%, with the 5 wt% loading showing enhanced material properties compared with the 2.5 wt%, due to particle reinforcement in the composite. It was found that both batches exhibited a strong damage precursor detection ability, with a clear statistical difference in the fluorescence before compression and after 2% applied strain, increasing rapidly with increasing applied strain, until leveling off after 6% strain. In addition, the 5 wt% Di-AC batch had higher fluorescence overall, which is expected as the Di-AC has some intrinsic fluorescence, thus using more of the material would cause the initial fluorescence to also be increased. Overall, the synthesis of Di-AC as a stress-sensitive particle filler allows for facile addition of advanced functionality to these ubiquitous thermoset composites.

ACKNOWLEDGMENTS

We would like to acknowledge the Program Manager Dr. David Stepp from the Army Research Office, and student support from the National Science Foundation Graduate Research Fellowship Program, the ARCS Foundation, and the Fulton Undergraduate Research Initiative. We would also like to acknowledge the W. M. Keck Bioimaging Laboratory, the LeRoy Eyring Center for Solid State Science, and the Adaptive Intelligent Materials & Systems Center, all at Arizona State University, for facilities use.

REFERENCES

1. D. Oates, *World Archaeol*., **21**, 388 (1990).
2. S. Stankovich, D.A. Dikin, G.H.B. Dommett, K.M. Kohlhaas, E.J. Zimney, E.A. Stach, R.D. Piner, S.T. Nguyen, and R.S. Ruoff, *Nature*, **442**, 282 (2006).
3. B. Dabbousi, J. RodriguezViejo, F. Mikulec, J. Heine, H. Mattoussi, R. Ober, K. Jensen, and M. Bawendi, *J. Phys. Chem. B*, **101**, 9463 (1997).
4. W. Sun, L. Chen, Y. Wang, Y. Zhou, S. Meng, H. Li, and Y. Luo, *Synth. React. Inorg. Met. Org. Nano-Metal Chem*., **46**, 437 (2016).
5. B. Zhang, F. Kang, J. Tarascon, and J. Kim, *Prog. Mater. Sci*., **76**, 319 (2016).
6. Q. Nadeem, M. Rizwan, R. Gill, M. Rafique, and M. Shahid, *J. Appl. Polym. Sci*., **133**, 42939 (2016).
7. N. Bouazizi, F. Ajala, A. Bettaibi, M. Khelil, A. Benghnia, R. Bargougui, S. Louhichi, L. Labiadh, R. Ben Slama, B. Chaouachi, K. Khirouni, A. Houas, and A. Azzouz, *J. Alloys Compd*., **656**, 146 (2016).
8. L. Hench, *J. Am. Ceram. Soc*., **81**, 1705 (1998).
9. E. Sackmann, *Science*, **271**, 43 (1996).
10. M.M. Farid, L. Goudini, F. Piri, A. Zamani, and F. Saadati, *Food Chem*., **194**, 61 (2016).
11. S. Banerjee and K.K. Kar, *J. Appl. Polym. Sci*., **133**, 42952 (2016).
12. W. Chang and H. Chen, *Food Hydrocoll*., **53**, 75 (2016).
13. M. Ulbricht, *Polymer*, **47**, 2217 (2006).
14. M. Haruta, *Catal. Today*, **36**, 153 (1997).
15. L.N. Bobrova, A.S. Bobin, N.V. Mezentseva, V.A. Sadykov, J.W. Thybaut, and G.B. Marin, *Appl. Catal. B*, **182**, 513 (2016).
16. X. Song, Y. Hu, M. Zheng, and C. Wei, *Appl. Catal. B*, **182**, 587 (2016).
17. Y. Yuan, Z. Yu, Y. Li, H. Lu, X. Chen, W. Tu, Z. Ji, and Z. Zou, *Appl. Catal. B: Environ*., **181**, 16 (2016).
18. G. Yu, J. Gao, J.C. Hummelen, F. Wudl, and A.J. Heeger, *Science*, **270**, 1789 (1995).
19. S.H. Park, A. Roy, S. Beaupre, S. Cho, N. Coates, J.S. Moon, D. Moses, M. Leclerc, K. Lee, and A.J. Heeger, *Nat. Photonics*, **3**, 297 (2009).
20. B.C. Thompson and J.M.J. Frechet, *Angew. Chem. Int. Ed*., **47**, 58 (2008).
21. P.G. Bruce, B. Scrosati, and J. Tarascon, *Angew. Chem. Int. Ed*., **47**, 2930 (2008).
22. J.Y. Kim, K. Lee, N.E. Coates, D. Moses, T. Nguyen, M. Dante, and A.J. Heeger, *Science*, **317**, 222 (2007).
23. J. Rowsell and O. Yaghi, *Angew. Chem. Int. Ed*., **44**, 4670 (2005).
24. K.A. Simon, N.J. Warren, B. Mosadegh, M.R. Mohammady, G.M. Whitesides, and S.P. Armes, *Biomacromolecules*, **16**, 3958 (2015).
25. G.A. Bagheri, *J. Alloys Compd*., **676**, 120 (2016).
26. H.J. Boehm and A. Rasool, *Int. J. Solids Struct*., **87**, 90 (2016).
27. A. Boonyapookana, A. Saengsai, S. Surapunt, K. Nagata, and Y. Mutoh, *Int. J. Fatigue*, **87**, 288 (2016).
28. A.L. Yesgat and R. Kitey, *Eng. Fract. Mech*., **160**, 22 (2016).
29. L. Takacs, *Acta Phys. Pol. A*, **121**, 711 (2012).
30. C.R. Hickenboth, J.S. Moore, S.R. White, N.R. Sottos, J. Baudry, and S.R. Wilson, *Nature*, **446**, 423 (2007).
31. P. Michael and W.H. Binder, *Angew. Chem. Int. Ed*., **54**, 13918 (2015).
32. M.B. Larsen and A.J. Boydston, *Macromol. Chem. Phys*., **213**, 354 (2016).
33. S.M. Avdoshenko and D.E. Makarov, *J. Phys. Chem. B*, **120**, 1537 (2016).
34. Y. Chen, A.J.H. Spiering, S. Karthikeyan, G.W.M. Peters, E.W. Meijer, and R.P. Sijbesma, *Nat. Chem*., **4**, 559 (2012).
35. A.L.B. Ramirez, A.K. Schmitt, M.K. Mahanthappa, and S.L. Craig, *Faraday Discuss*., **170**, 337 (2014).
36. H. Zhang, F. Gao, X. Cao, Y. Li, Y. Xu, W. Weng, and R. Boulatov, *Angew. Chem. Int. Ed*., **55**, 3040 (2016).
37. M.J. Jacobs, G. Schneider, and K.G. Blank, *Angew. Chem. Int. Ed*., **55**, 2899 (2016).
38. Y. Sagara, Y.C. Simon, N. Tamaoki, and C. Weder, *Chem. Commun*., **52**, 5694 (2016).
39. S. Cho, J. Kim, and C. Chung, *Sens. Actuators B*, **134**, 822 (2008).
40. S. Cho, J. Kim, and C. Chung, *J. Nanosci. Nanotechnol*., **10**, 6972 (2010).
41. C. Chung, Y. Roh, S. Cho, and J. Kim, *Chem. Mat*., **16**, 3982 (2004).
42. Z.S. Kean, Z. Niu, G.B. Hewage, A.L. Rheingold, and S.L. Craig, *J. Am. Chem. Soc*., **135**, 13598 (2013).

 DOI 10.1002/pen

43. J.M. Lenhardt, A.L. Black, and S.L. Craig, *J. Am. Chem. Soc*., **131**, 10818 (2009).
44. A.L.B. Ramirez, Z.S. Kean, J.A. Orlicki, M. Champhekar, S.M. Elsakr, W.E. Krause, and S.L. Craig, *Nat. Chem*., **5**, 757 (2013).
45. Z. Ma, F. Yang, Z. Wang, and X. Jia, *Tetrahedron Lett*., **56**, 393 (2015).
46. S.B. Brichkin, V.F. Razumov, L.M. Bogdanova, and B.A. Rozenberg, *Polym. Sci. Ser. A*, **42**, 516 (2000).
47. Y. Sagara, S. Yamane, T. Mutai, K. Araki, and T. Kato, *Adv. Funct. Mater*., **19**, 1869 (2009).
48. T. Defize, R. Riva, C. Jerome, and M. Alexandre, *Macromol. Chem. Phys*., **213**, 187 (2012).
49. P. Froimowicz, H. Frey, and K. Landfester, *Macromol. Rapid Commun*., **32**, 468 (2011).
50. Y. Song, K. Lee, W. Hong, S. Cho, H. Yu, and C. Chung, *J. Mater. Chem*., **22**, 1380 (2012).
51. F. Tong, C.D. Cruz, S.R. Jezowski, X. Zhou, L. Zhu, R. Al-Kaysi, E.L. Chronister, and C.J. Bardeen, *J. Phys. Chem. A*, **118**, 5379 (2014).
52. S.R. Jezowski, L. Zhu, Y. Wang, A.P. Rice, G.W. Scott, C.J. Bardeen, and E.L. Chronister, *J. Am. Chem. Soc*., **134**, 7459 (2012).
53. G.R. Gossweiler, G.B. Hewage, G. Soriano, Q. Wang, G.W. Welshofer, X. Zhao, and S.L. Craig, *ACS Macro Lett*., **3**, 216 (2014).
54. N. Yoshie, S. Saito, and N. Oya, *Polymer*, **52**, 6074 (2011).
55. J. Xing, M. Zheng, W. Chen, X. Dong, N. Takeyasu, T. Tanaka, Z. Zhao, X. Duan, and S. Kawata, *Phys. Chem. Chem. Phys*., **14**, 15785 (2012).
56. D.A. Davis, A. Hamilton, J. Yang, L.D. Cremar, D. Van Gough, S.L. Potisek, M.T. Ong, P.V. Braun, T.J. Martinez, S.R. White, J.S. Moore, and N.R. Sottos, *Nature*, **459**, 68 (2009).
57. C.K. Lee, B.A. Beiermann, M.N. Silberstein, J. Wang, J.S. Moore, N.R. Sottos, and P.V. Braun, *Macromolecules*, **46**, 3746 (2013).
58. Y. Chen and R.P. Sijbesma, *Macromolecules*, **47**, 3797 (2014).
59. M.B. Larsen and A.J. Boydston, *J. Am. Chem. Soc*., **136**, 1276 (2014).
60. K. Imato, T. Kanehara, T. Ohishi, M. Nishihara, H. Yajima, M. Ito, A. Takahara, and H. Otsuka, *ACS Macro Lett*., **4**, 1307 (2015).
61. Z. Wang, Z. Ma, Y. Wang, Z. Xu, Y. Luo, Y. Wei, and X. Jia, *Adv. Mater*., **27**, 6469 (2015).
62. J. Zou, Y. Liu, B. Shan, A. Chattopadhyay, and L.L. Dai, *Smart Mater. Struct*, **23**, 095038 (2014).
63. E.M. Nofen, J. Wickham, B. Koo, A. Chattopadhyay, and L.L. Dai, *Mater. Res. Express*, **3**, 035701 (2016).
64. Y. Ito and G. Olovsson, *J. Chem. Soc. Perkin Trans*., **1**, 127 (1997).
65. S. Hirose, T. Hatakeyama, and H. Hatakeyama, *Netsu Sokutei*, **30**, 154 (2003).
66. S. Hirose, T. Hatakeyama, and H. Hatakeyama, *Macromol. Symp*., **224**, 343 (2005).
67. L.E. Nielsen, *J. Macromol. Sci. Rev. Macromol. Chem*., **C3**, 69 (1969).
68. R. Auvergne, S. Caillol, G. David, B. Boutevin, and J. Pascault, *Chem. Rev*., **114**, 1082 (2014).